16

Correlation Coefficients of Received Signal I and Q Components in a Domain with Time and Frequency Axes under Multipath Mobile Channel with LOS and NLOS

Shigeru Kozono, Kenji Ookubo, Takeshi Kozima
and Tomohiro Hamashima
Department of Electrical, Electronics and Computer Engineering,
Chiba Institute of Technology
2-17-1 Tsudanuma, Narashino-shi, 275-0016,
Japan

1. Introduction

To support realtime multimedia communication, future mobile communications will require a high-bit-rate transmission system with high utilization of the frequency spectrum in very rich multipath channels [1]. Systems capable of fulfilling this requirement, with features such as orthogonal frequency division multiplexing (OFDM) [2], [3] and multiple-input multiple-output (MIMO) [4]–[7], have been studied extensively. Furthermore, the use of M-ary quadrature amplitude modulation (M-ary QAM) with coherent detection helps to meet the transmission requirements. Such systems overcome frequency selective fading by using a narrowband multiple-carrier signal called a sub-channel. Those systems use sophisticated and refined techniques and several of those techniques are usually combined in one system. To make full use of the techniques in the system design and achieve high-quality transmission, we must design a system taking into consideration wide and detailed multipath properties in a domain with time and frequency axes. OFDM works best with a lot of narrow bands for the sub-channel. MIMO also requires multipath properties between the antennas composing the MIMO antenna, and it requires a low correlation coefficient. M-ary QAM detection also requires the device to compensate accurately for both the in-phase and quadrature (I and Q) components of the sub-channel for the ever-changing multipath channel associated with terminal movement, and this is achieved by putting a pilot signal in the information data [8].

Figure 1 shows an example of the sub-channel state of the I and Q components and phase ψ ($\tan^{-1}(Q/I)$) as movement in a multipath channel, and Fig. 2 shows the signal state diagram at the moment. With movement, the I, Q, and the phase ψ change irregularly as shown by solid lines in Fig.1, so we cannot use the sub-channel as a transmission line. Therefore, the sub-channel needs to be a stable state with compensation by a pilot signal. The states of the sub-channel compensated every $10T_{sy}$ (T_{sy}: symbol length) in information data, which

corresponds to a 0.1λ [m] running distance, are shown by broken lines in Fig. 1, the I and Q components become stable, and the sub-channel can then be used as a transmission line. This phenomenon in Fig. 2 appears as concentrated points in a small broken circle, so it is possible that a received signal with M-ary QAM is detected. The pilot signal is inserted at a fixed interval in information data: in particular the pilot signal in a combined system with OFDM and M-ary QAM is allocated in a domain with time and frequency axes and there must be a high correlation coefficient between pilot signals. This signal allocation is very important because it influences transmission efficiency and bit error rate (BER).

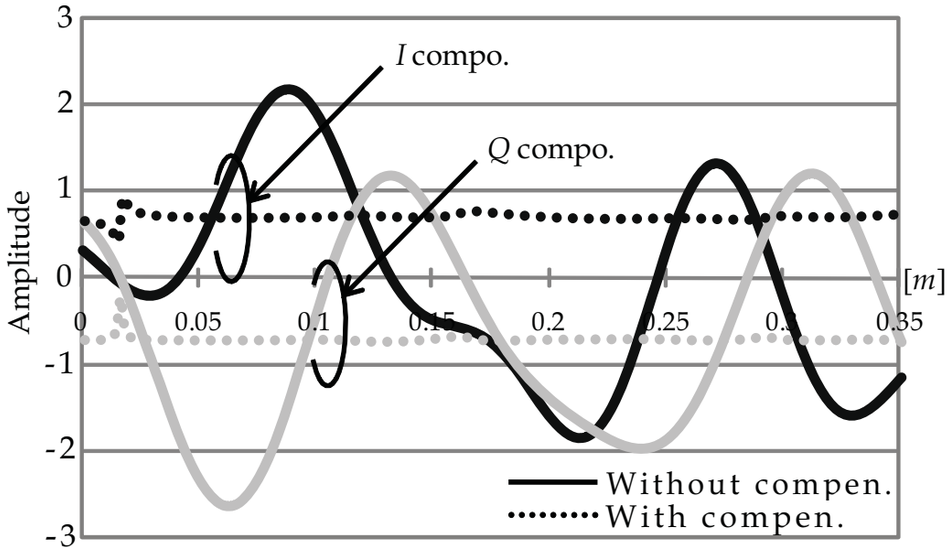

(a) I and Q components

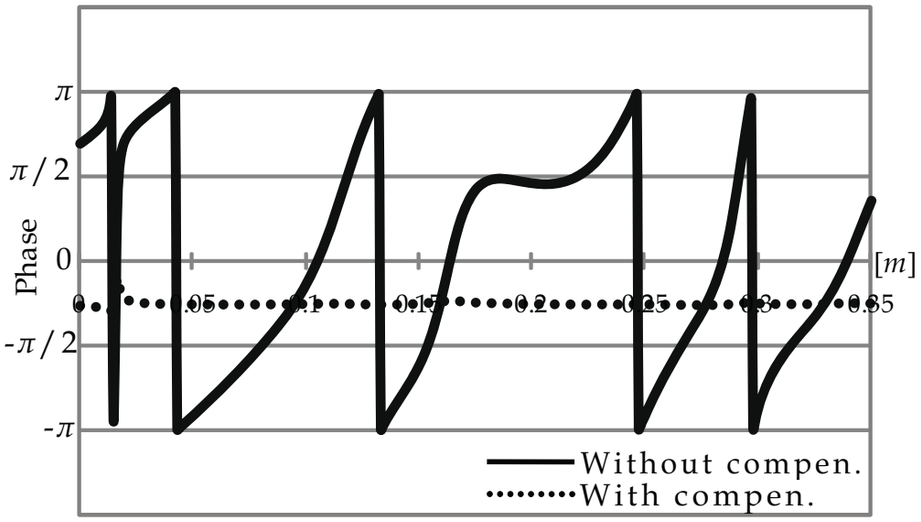

(b) Phase ψ

Fig. 1. Example of sub-channel variations with movement

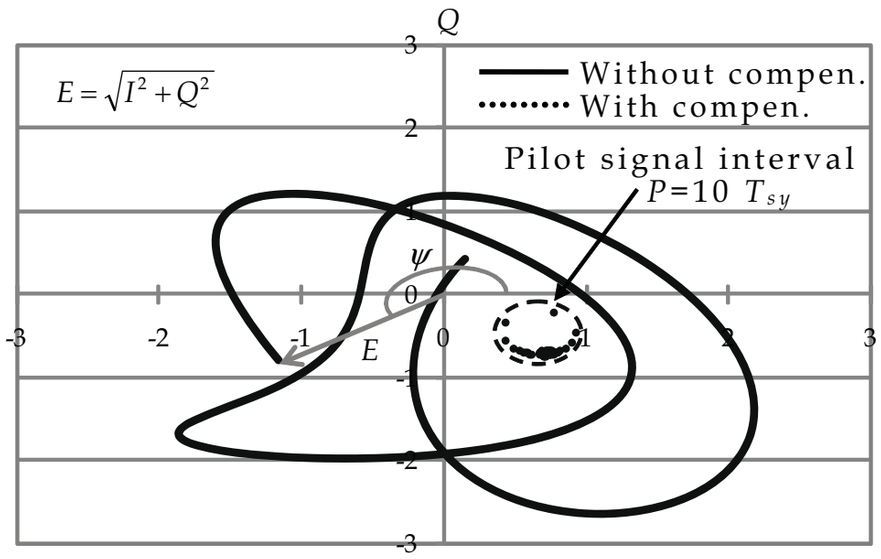

Fig. 2. Signal state diagram with I and Q components in Fig. 1

What the wireless system design requires in terms of basic multipath properties seems to be the correlation of the sub-channel's I and Q components in a domain with time and frequency axes. Many theoretical and experimental studies have been performed on the correlation of received signal amplitudes [9]–[12], but the correlation of the I and Q components has hardly been studied at all [9]. Furthermore, the ordinary formula for amplitude correlation given by Jakes [10] is derived on the basis of the I and Q components with a random Gaussian variable in the non-line-of-sight (NLOS) condition. With this in mind, we paid attention to the delay profile with actual multipath data in a mobile channel and developed an analysis model with a domain having time, frequency, and space (delay time) axes to investigate the correlation using the profile [13]. Furthermore, we derived a correlation formula for various profile types for the line-of-sight (LOS) and NLOS conditions and also verified the theory by computer simulation.

This chapter is organized as follows. Section 2 describes a propagation model and analysis model. Section 3 covers the theoretical study. First, we derive the general correlation formula for the I and Q components using a delay profile for LOS or NLOS. Next as examples, we derived formulas for delay profiles when the arriving wave has an exponentially decreasing amplitude and a random amplitude. Section 4 covers simulation. The simulation method and parameters are described and the simulation results are presented. The simulation was done for autocorrelation and for frequency correlation on time and frequency axes for LOS and NLOS and also done in the domain for those profiles. Then, the correlation formulas were evaluated. Finally, section 5 summarizes the results.

2. Propagation model and analysis model

A. Propagation model

In a mobile radio channel, numerous waves arrive at a receiving point via multiple paths, with each wave having a certain amplitude, a certain delay time, and a random arrival angle. Consequently, the arriving waves interfere with each other and standing waves are

produced. Thus, the received signal amplitude varies with terminal movement and has a Rayleigh or Nakagami-Rice distribution. An example of the delay profile is shown in Fig. 3 for the following conditions.

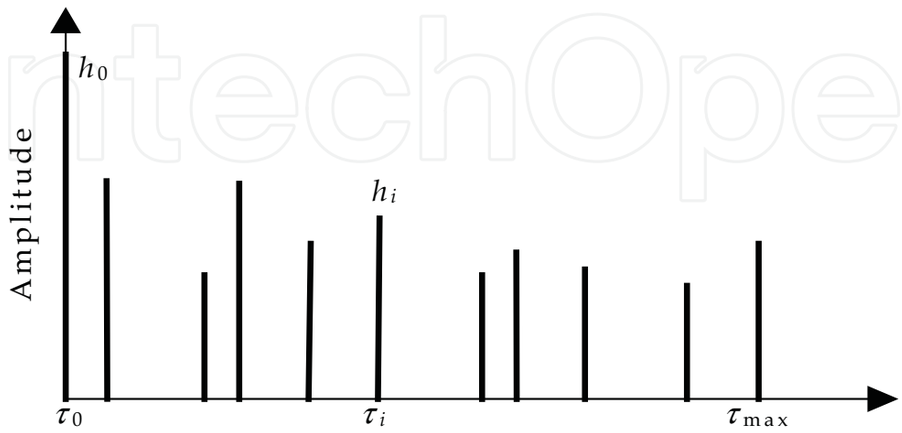

Fig. 3. Example of delay profile

i. The number of arriving waves is N+1, the waves are independent of each other, and the ith arriving wave is denoted by subscript i, where i=0 means a directive wave and i≥1 means no directive waves.
ii. The waves have an excess delay time τ_i relative to the directive wave and a maximum excess delay time τ_{max}. The τ_i values are random from τ_0 to τ_{max}.
iii. The amplitude is h_i, the power ratio of the directive and nondirective waves is denoted by k (K: in dB), and k=0 (K=-∞ dB) means NLOS. Furthermore, the nondirective wave's power is normalized to 1.
iv. The arrival angle is ξ_i, the initial phase is ϕ_i, and the values are random from 0 to 2π rad.

B. Multipath channel

Under the above conditions, the envelope $\dot{E}(t, f_c)$ of a received signal is given by (1), where $I(t, f_c)$ and $Q(t, f_c)$ express the in-phase (real) and quadrature (imaginary) components of $\dot{E}(t, f_c)$, respectively.

$$\dot{E}(t, f_c) = \sum_{i=0}^{N} h_i e^{j\theta_i}$$

$$= I(t, f_c) + jQ(t, f_c) \tag{1}$$

$$I(t, f_c) = \sum_{i=0}^{N} h_i \cos\theta_i \tag{2-a}$$

$$Q(t, f_c) = \sum_{i=0}^{N} h_i \sin\theta_i \tag{2-b}$$

$$\theta_i = 2\pi(f_c\tau_i - f_m t\cos\xi_i) + \phi_i \tag{3}$$

Here, θ_i is the path phase of the ith arriving wave, f_c is the radio frequency, and f_m is the maximum fading frequency calculated as v/λ, where v is the moving speed and λ is the wavelength. As shown by (2) and (3), the I and Q components are functions of variable θ_i, which is a function of f_c, t, and v, for a given delay profile. When the sub-channel bandwidth of the system, such as an OFDM system, is f_0, we have $f_c >> f_0$ since we treat a narrowband channel in a multipath environment. Therefore, we treat the frequency separately from f_c as $\Delta f = nf_0$ (n: integer). Figure 4 shows an example of an OFDM channel with a lot of sub-channels in a domain with time (vt) and frequency (nf_0): each sub-channel amplitude $|E(t, f_c)|$ changes severely and deeply in the domain.

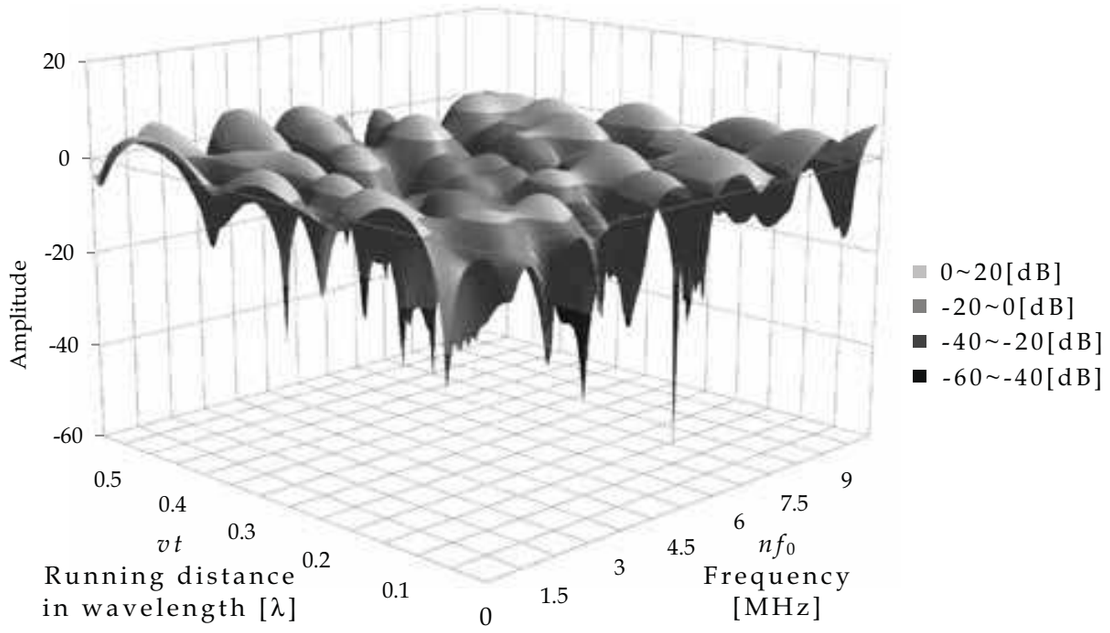

Fig. 4. Example of OFDM channel in multipath condition

C. Analysis model

As shown (2), the $I(t, f_c)$ and $Q(t, f_c)$ depend on θ_i by (3) for a given delay profile and the θ_i is a function of $f_c\tau_i$ and $f_m t$. Therefore, we study the correlation of $I(t, f_c)$ and $Q(t, f_c)$ by using the variables of $f_m T_s$ (normalized maximum Doppler frequency) on the time axis and $\Delta f\sigma$ (σ: delay spread) on the frequency axis. For example, T_s is absolute time t minus relative time T_0 for a directive wave arriving at the receiving point, i.e., $T_s = t - T_0$; Δf is the frequency separation from the radio frequency f_c, i.e., $\Delta f = f - f_c$. Furthermore, to simplify the expression of those variables, we introduce $x = f_m T_s + \Delta f\sigma$ as a variable of time and frequency. Moreover, we choose the origin $P_0(0,0)$ and the point under consideration for the correlation $P_1(f_m T_s, \Delta f\sigma)$ to correspond to $x=0$ and $x=\Delta x$, respectively. Consequently, those points are expressed by $P_0(0)$ and $P_1(\Delta x)$, and we can calculate the correlation coefficient $\rho(\Delta x)$ as the correlation between $P_0(0)$ and $P_1(\Delta x)$. We denote the correlation coefficients for the I and Q components using the

symbols $\rho_I(\Delta x)$ and $\rho_Q(\Delta x)$, respectively. The path phases of the ith arriving wave θ_i given by (3) at $P_0(0)$ and $P_1(\Delta x)$ are also represented by (4-a) and (4-b), respectively.

$$\theta_i(0) = 2\pi f_c \tau_i + \phi_i, \tag{4-a}$$

$$\theta_i(\Delta x) = 2\pi((f_c + \Delta f)\tau_i - f_m T_s \cos\xi_i) + \phi_i \tag{4-b}$$

3. Derivation of correlation coefficients

A. General formula derivation

We start by studying the correlation coefficient of the I component. With the variable x, the correlation coefficient of the I component is generally expressed by

$$\rho_I(\Delta x) = \frac{\langle (I(0)I(\Delta x)\rangle - \langle I(0)\rangle\langle I(\Delta x)\rangle}{[\{< (I(0))^2 > - < I(0) >^2\}\{< (I(\Delta x))^2 > - < I(\Delta x) >^2\}]^{1/2}}. \tag{5}$$

Here, the symbol < > means an ensemble average. Under the conditions of the propagation model in 2-*A* and assuming that N is a large of number, we can start to calculate each term in (5).

First, we calculate the terms $<I(0)>$ and $<I(\Delta x)>$. Because τ_i, ξ_i, and ϕ_i have random values, the ensemble averages at x=0 and Δx become zero when (4-a) and (4-b) are used to substitute for θ_i in (2-a), so these terms become

$$\langle I(0)\rangle = \langle I(\Delta x)\rangle = 0. \tag{6}$$

Second, we calculate $<I(0)^2>$ and $<I(\Delta x)^2>$. Though the ensemble averages for the product of different ith arriving waves vanish since τ_i, ξ_i, and ϕ_i have random values, those of the same ith arriving waves remain as the power, and we get

$$\langle I(0)^2\rangle = \langle I(\Delta x)^2\rangle = \frac{1}{2}\langle\sum_{i=0}^{N} h_i^2\rangle. \tag{7}$$

Next, we calculate the term $<I(0)I(\Delta x)>$. When we consider τ_i, ξ_i, and ϕ_i to be random values and take an odd function of sine, this term becomes as follows (see appendix A).

$$\langle I(0)I(\Delta x)\rangle = \frac{1}{2}\langle\sum_{i=0}^{N} h_i^2 \cos(2\pi\Delta f\tau_i)\cos(-2\pi f_m' T_s \cos\xi_i)\rangle \tag{8}$$

Through (6) to (8), we can calculate the denominator and numerator in (5). Both $\langle I(0)^2\rangle - \langle I(0)\rangle^2$ and $\langle I(\Delta x)^2\rangle - \langle I(\Delta x)\rangle^2$ in the denominator are $\frac{1}{2}\langle\sum_{i=0}^{N} h_i^2\rangle$ by (7) minus (6), so the denominator is $\frac{1}{2}\langle\sum_{i=0}^{N} h_i^2\rangle$. On the other hand, the numerator becomes $\frac{1}{2}\langle\sum_{i=0}^{N} h_i^2 \cos(2\pi\Delta f\tau_i)\cos(-2\pi f_m' T_s \cos\xi_i)\rangle$ by (6) and (8). Finally, we can rewrite correlation coefficient $\rho_I(\Delta x)$ in (5) as (9).

$$\rho_I(\Delta x) = \frac{\frac{1}{2}\langle \sum_{i=0}^{N} h_i^2 \cos(2\pi\Delta f \tau_i)\cos(-2\pi f_m' T_s \cos\xi_i) \rangle}{\frac{1}{2}\langle \sum_{i=0}^{N} h_i^2 \rangle} \tag{9}$$

Equation (9) represents a general correlation coefficient formula for the I component, and it is applicable to a delay profile for both LOS and NLOS conditions.

Next, we study the correlation coefficient of the Q component. It is easy to understand that the correlation coefficient of the Q component is given by the same formula (9) as that for the I component. The reason is as follows. Since (9) does not contain ϕ_i, we can replace ϕ_i in (3) by $\phi_i + \pi/2$ and substitute $\phi_i + \pi/2$ for ϕ_i in θ_i for $\sin\theta_i$ in (2-b). Consequently, the term $\sin\theta_i$ becomes $\cos\theta_i$ analytically, and the properties of $Q(t, f_c)$ then become statistically similar to those of $I(t, f_c)$. Thus, since we can calculate the correlation coefficients of both the I and Q components by using the I component, from here on we treat only the I component, which we denote simply as $\rho(\Delta x)$.

B. Correlation coefficient in given delay profile

i) Type 1: *Delay profile with exponential distribution*

We first calculate correlation coefficient $\rho(\Delta x)$ in (9) for a delay profile with an exponential distribution, as shown in Fig. 5(a). It has a directive wave with amplitude h_0 and excess delay time τ_0=0 and also has a lot of nondirective waves for which h_i decreases exponentially according to (10) as excess delay time τ_i increases.

$$h_i = h\exp(-\tau_i/\tau_{av}) \ , \tag{10}$$

where h is the amplitude at τ_i=0 and τ_{av} is the average excess delay time. Under this condition and for the propagation model in 2-*A*, we analytically derive the correlation coefficient formula on the basis of $\rho(\Delta x)$ in (9). The denominator in (9) is k+1 because the power of the nondirective wave was normalized to 1. Furthermore, since τ_i and ξ_i are independent, the numerator in (9) can be separated into two parts, A_1 and B_1, as in (11).

$$A_1 B_1 = \langle \frac{1}{2}\sum_{i=0}^{N} h_i^2 \cos(2\pi\Delta f \tau_i)\rangle \langle \sum_{i=0}^{N} \cos(-2\pi f_m' T_s \cos\xi_i)\rangle \tag{11}$$

When N is a large number, $\tau_{\max}$ is large, and h_i decreases according to (10), the first term A_1 can be calculated by integrating with respect to τ. As shown in appendix *B*, it becomes

$$\begin{aligned} A_1 &= \langle \frac{1}{2} h_0^2 \rangle + \frac{1}{2}\int_{\tau_{\min}}^{\tau_{\max}} h^2 \exp(-2\tau/\tau_{av})\cos(2\pi\Delta f \tau) d\tau \\ &= k + \frac{1}{1+(2\pi\Delta f)^2(\tau_{av}/2)^2}. \end{aligned} \tag{12}$$

Concerning the second part, B_1, it is well known that $B_1 = J_0(2\pi f_m' T_s)$, where $J_0(\bullet)$ is a zeroth-order Bessel function of the first kind and f_m' is the maximum fading frequency at $f_c + \Delta f$. Moreover, the value of $\tau_{av}/2$ in (12) is equal to delay spread σ when $\tau_{\max}$ is very large and h_i becomes very small at $\tau_{\max}$. Replacing $2\pi\Delta f$ by s, we finally get the correlation coefficient $\rho(\Delta x)$.

$$\rho(\Delta x) = \frac{k + 1/(1+s^2\sigma^2)}{k+1} J_0(2\pi f_m' T_s) \tag{13}$$

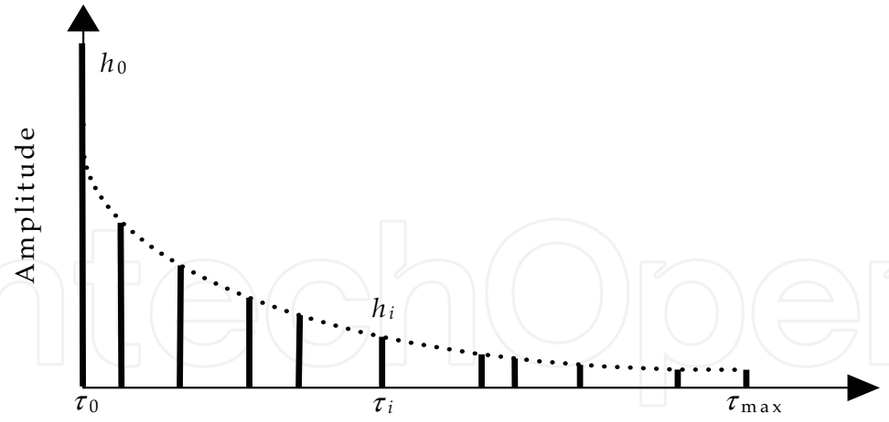

(a) Exponential distribution

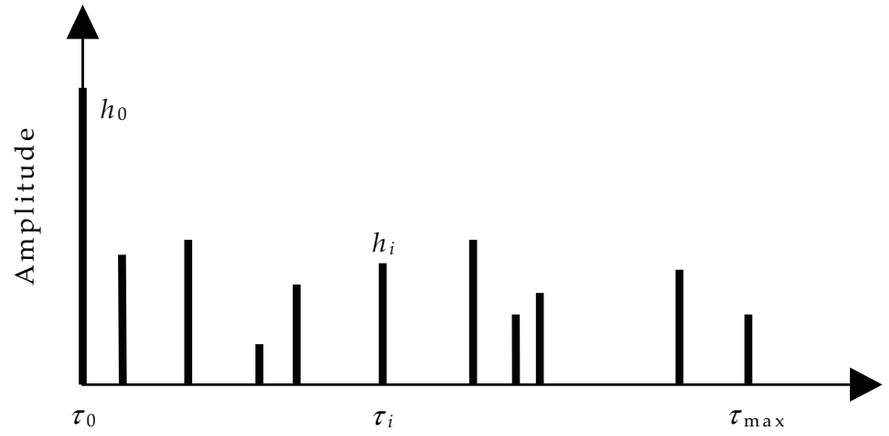

(b) Random distribution

Fig. 5. Delay profile used formula derivation

ii) Type 2: *Delay profile with random distribution*

Next, we calculate the correlation $\rho(\Delta x)$ for a delay profile with a random distribution, as shown in Fig. 5(b). It has a directive wave and a lot of nondirective waves like Fig. 5(a), but h_i and τ_i of the nondirective waves are independent. Excess delay time τ_i has maximum value τ_{max} and is random between τ_{min} (close to 0) and τ_{max}. In a similar way to that for type 1, the denominator in (9) is also k+1, and the numerator in (9) can also be separated into A_2 and B_2; moreover, A_2 separates into directive and nondirective waves, as shown in (14).

$$A_2 B_2 = \langle \frac{1}{2} h_0^2 + \frac{1}{2} \sum_{i=1}^{N} h_i^2 \cos(2\pi \Delta f \tau_i) \rangle \langle \sum_{i=0}^{N} \cos(-2\pi f_m' T_s \cos \xi_i) \rangle \tag{14}$$

In the first ensemble average in (14), the power of a directive wave is k and that of a nondirective one is 1; moreover, h_i and τ_i are independent. Therefore, A_2 becomes (15) by a similar integration to that for type 1 (see appendix C).

$$A_2 = \langle k + \sum_{i=1}^{N} \cos(2\pi \Delta f \tau_i) \rangle \quad = k + \frac{\sin(2\pi \Delta f \tau_{max})}{2\pi \Delta f \tau_{max}} \tag{15}$$

B_2 in (14) also becomes $J_0(2\pi f_m' T_s)$. From the above description, the correlation coefficient $\rho(\Delta x)$ becomes

$$\rho(\Delta x) = \frac{k + \sin(2\pi\Delta f \tau_{\max}) \Big/ 2\pi\Delta f \tau_{\max}}{k+1} J_0(2\pi f_m' T_s). \tag{16}$$

From (13) and (16), the autocorrelation on the time axis is independent of the delay profile and always seems to be a zeroth-order Bessel function of the first kind, $J_0(\bullet)$, whenever arriving angle ξ_i has a uniform distribution over 0 to 2π. However, the frequency correlation on the frequency axis depends on whether the delay profile is for LOS or NLOS and whether it is dependent on or independent of h_i and τ_i.

4. Simulation

A. Simulation method

A computer simulation was performed to verify the correlation coefficient formula derived in 3-*B*. The simulation parameters are listed in Table 1.

Frequency f_c	2 GHz
Number of arriving waves N +1	10+1
Nakagami-Rice factor K	-∞, 5 dB
Average excess delay time τ_{av} Maximum excess delay time $\tau_{\max}$	1 μs (type 1) 2 μs (type 2)
Effective amplitude h_i	-20 dB

Table 1. Simulation parameters

Simulation was done to confirm (13) for type 1 with an exponential distribution and (16) for type 2 with a random distribution, and it mainly simulated correlations such as autocorrelation on the time axis, frequency correlation on the frequency axis, and correlation in a domain with time and frequency axes. The correlation was simulated by using the delay profile in actually and frequently encountered environments within the propagation model in 2-*A*, such that N was 10, the effective amplitude of arriving wave was -20 dB relative to the maximum for a nondirective wave, and the K factor took values of -∞ and 5 dB. For type 1, the average delay time τ_{av} was 1 μs when the statistical delay spread σ was about 0.42 μs at K= -∞ dB. For type 2, the maximum delay time $\tau_{\max}$ was 2 μs and σ was 0.50 μs. The simulation was performed on the basis of (2) and (5). Each simulated value of $\rho(\Delta x)$ was calculated from an ensemble average for more than 10^6 delay profiles. Thus, we performed a statistical analysis in the simulation.

B. Simulation results and considerations

i) Type 1: Delay profile with exponential distribution

Figure 6 shows the correlation coefficient simulated using a delay profile with exponential distributions of K=-∞ and 5 dB denoted by symbols × and ▲, respectively. Figures 6(a) and

(b) are the correlations on the time and frequency axes, i.e., the well known autocorrelation and frequency correlation, respectively. In Fig. 6(a), the fine line is the theoretical value of $\rho(\Delta x)$ obtained from (13) by putting Δf =0 or $\rho(\Delta x)=J_0(2\pi f'_m T_s)$. The simulated autocorrelations for both K=-∞ and 5 dB have almost the same features and agree with the theoretical value. This shows that the autocorrelation is independent of the K factor and is expressed by $J_0(2\pi f'_m T_s)$. In Fig. 6(b), the fine and broken lines are theoretical values of $\rho(\Delta x)$ obtained from (13) by putting $f'_m T_s$=0 or $\frac{k+1/(1+s^2\sigma^2)}{k+1}$. Here, we note that delay spread σ was calculated for NLOS without any directive waves. The frequency correlations for K=-∞ and 5 dB have different features, so the correlation depends on the K factor. The simulated

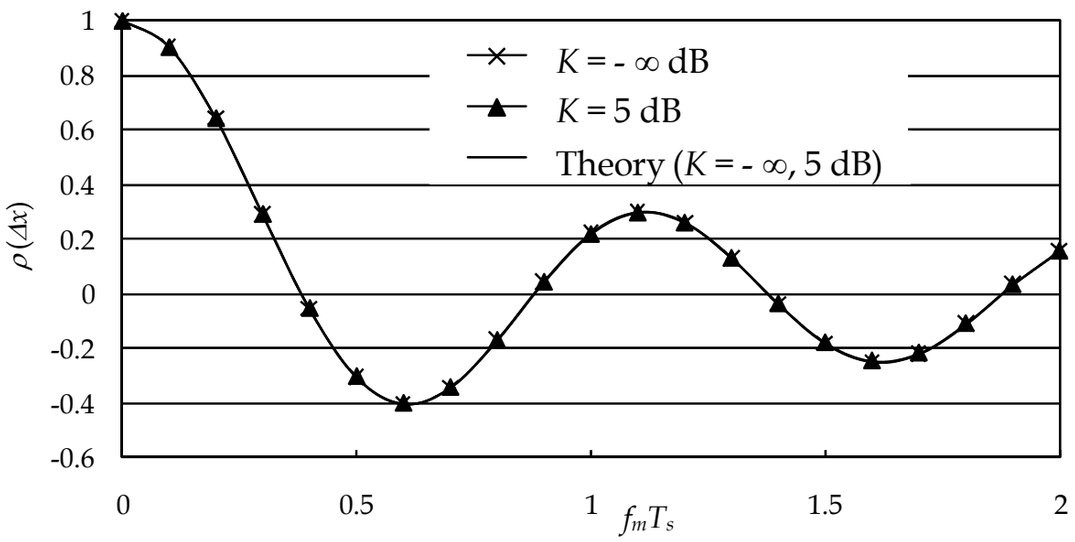

(a) Autocorrelation

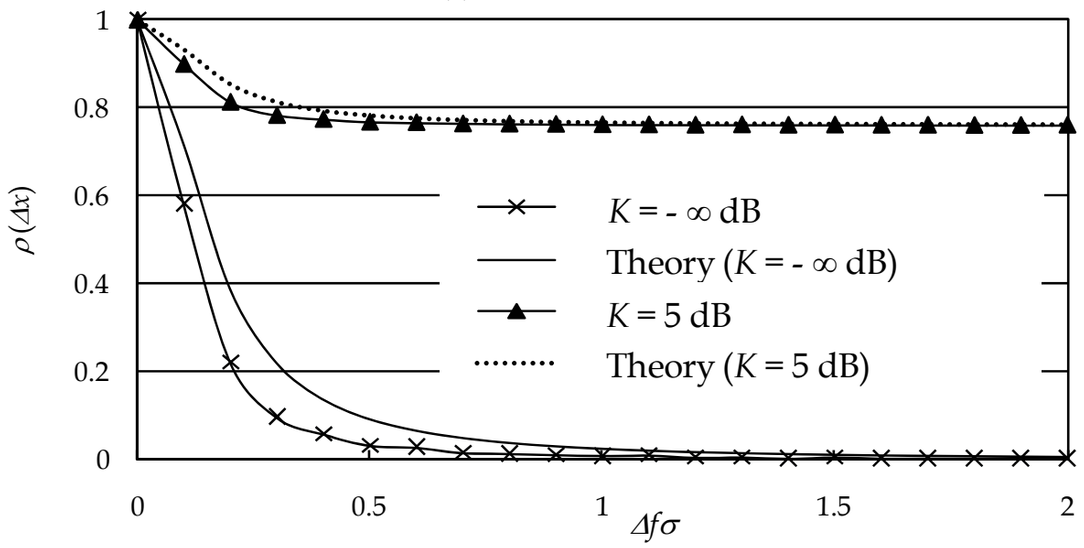

(b) Frequency correlation

Fig. 6. Correlation coefficient (Type 1: exponential distribution)

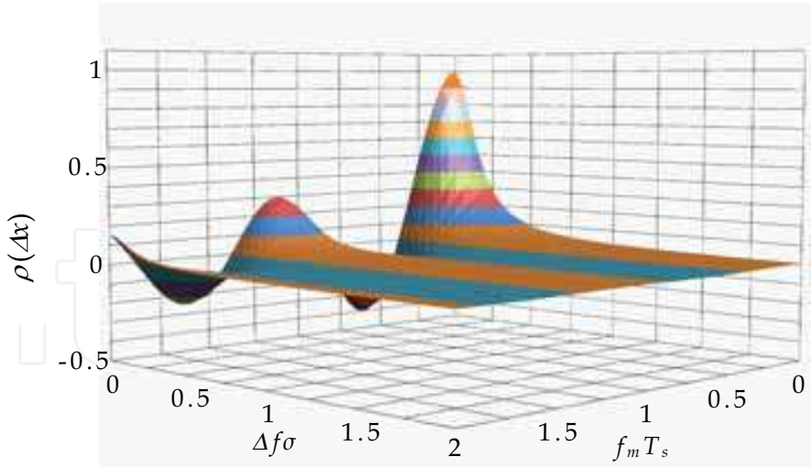

(a) Bird's-eye view (theory)

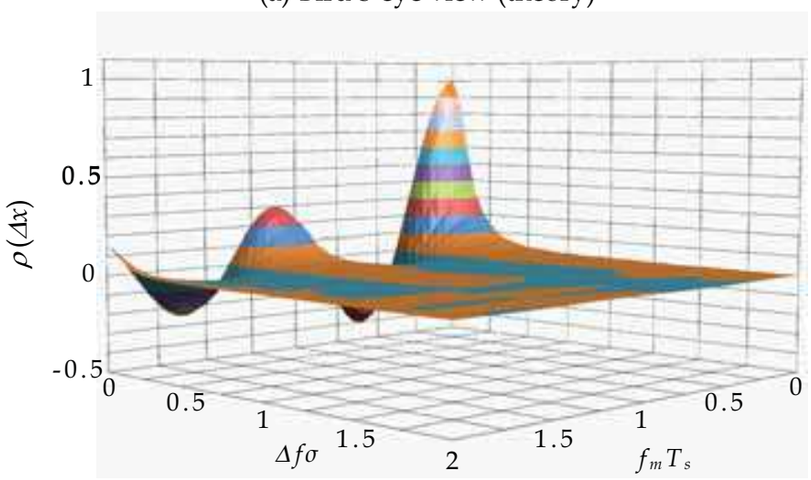

(b) Bird's-eye view (simulation)

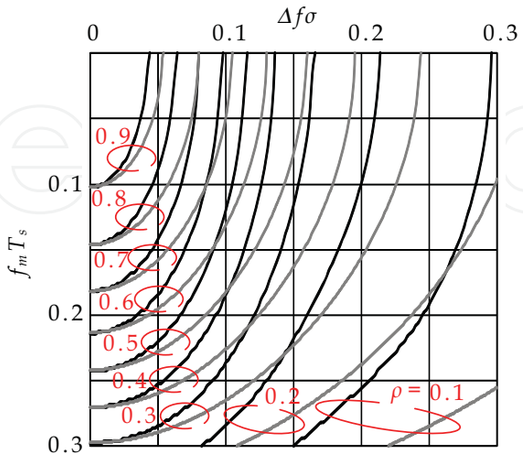

(c) Locus of theory (fine) & simulation(solid)

Fig. 7. Correlation coefficient in a domain with time and frequency axes
(Type 1: exponential distribution , K = -∞ dB)

correlation for K= -∞ dB is slightly lower than the theoretical one. We suppose that the difference is due to different conditions between the theoretical and simulation models for the delay profile, such as the number of waves N and the counted effective amplitude in h_i. Therefore, we repeated the simulation, changing from N=10 and effective amplitude of -20 dB to N>100 and effective amplitude of less than -50 dB. As a result, the correlation became close to the theoretical one. The above results show that the autocorrelation is independent of the K factor, while the frequency correlation depends on the K factor. The correlation coefficient in a domain with time and frequency axes for NLOS is shown in Fig. 7. Figure 7(a) is a bird's-eye view of $\rho(\Delta x)$ obtained from (13), which makes it easy to comprehend the overall $\rho(\Delta x)$. We can see that $\rho(\Delta x)$ has a peak $\rho(0)$=1 at the origin Δx = 0 and that $\rho(\Delta x)$ becomes smaller with increasing Δx or as $f'_m T_s$ and $\Delta f\sigma$ become larger. Furthermore, $\rho(\Delta x)$ decreases in a fluctuating manner on the time axis, but decreases monotonically on the frequency axis. The high area of $\rho(\Delta x)$ needed to allocate the pilot signal in coherent detection, such as $\rho(\Delta x)$ >0.8, is very small in the domain, whereas the low area needed to design the diversity antenna, such as $\rho(\Delta x)$ <0.5, is spread out widely. Figure 7(b) also shows a bird's-eye view of the simulated correlation; Figs. 7(a) and (b) both exhibit almost the same features. Figure 7(c) shows the loci of the theoretical and simulated correlations in a small area up to 0.3 on both axes, with contour lines of $\rho(\Delta x)$. It is easy to compare them. The theoretical value on the time axis agrees well with the simulated one, but the theoretical value on the frequency axis is slightly higher than the simulated one. The reason for this is a different model for the delay profile, as described earlier. We can see from Fig. 7(c) that the theoretical value agrees roughly with the simulated one. Furthermore, we note that in Fig. 7(c), the locus of the correlation coefficient $\rho(\Delta x)$ seems to be an ellipse with its major axis on the time axis and its origin Δx=0 in the domain.

ii) Type 2: Delay profile with random distribution

Figure 8 shows the correlation coefficient for a delay profile with random distributions of K=-∞ and 5 dB. The values plotted by symbols of × and ▲ in Figs. 8(a) and (b) were simulated in a similar way to Fig. 6, and the fine and broken lines show the theoretical value of $\rho(\Delta x)$ obtained from (16) by putting Δf =0 for autocorrelation or $\rho(\Delta x)=J_0(2\pi f'_m T_s)$ and by putting $f'_m T_s$=0 for frequency correlation or $\dfrac{k+\sin(2\pi\Delta f\tau_{\max})\big/2\pi\Delta f\tau_{\max}}{k+1}$. As shown in Fig. 8(a), the simulated autocorrelations for both K=-∞ and 5 [dB] have almost the same features and agree well with the theoretical values, so the correlation seems to be independent of the K factor. On the other hand, the simulated frequency correlations for K=-∞ and 5 dB in Fig. 8(b) have different features that also depend on the K factor. The simulated and theoretical values agree well.

The correlation coefficient in a domain with time and frequency axes for NLOS is shown in Fig. 9 by a similar method to that for Fig. 7. Figure 9(a) is a bird's-eye view of the theoretical value of $\rho(\Delta x)$ obtained from (16). We can also see that $\rho(\Delta x)$ has a peak $\rho(0)$=1 at the origin Δx = 0, and $\rho(\Delta x)$ becomes smaller with increasing Δx. However, in this case, $\rho(\Delta x)$ decreases in a fluctuating manner not only on the time axis, but also on the frequency axis. The high area of $\rho(\Delta x)$ in the domain, such as $\rho(\Delta x)$ >0.8, is larger than that for an exponential distribution; the low area, such as $\rho(\Delta x)$ <0.5, is spread out widely.

Figure 9(b) is the simulated correlation, which exhibits similar features to the theoretical one in Fig. 9(a). Figure 9(c) shows the loci of the theoretical and simulated correlations. The theoretical value in the domain agrees well with the simulated ones. For a delay profile with random distribution, the locus of correlation coefficient $\rho(\Delta x)$ is also an ellipse in the domain.

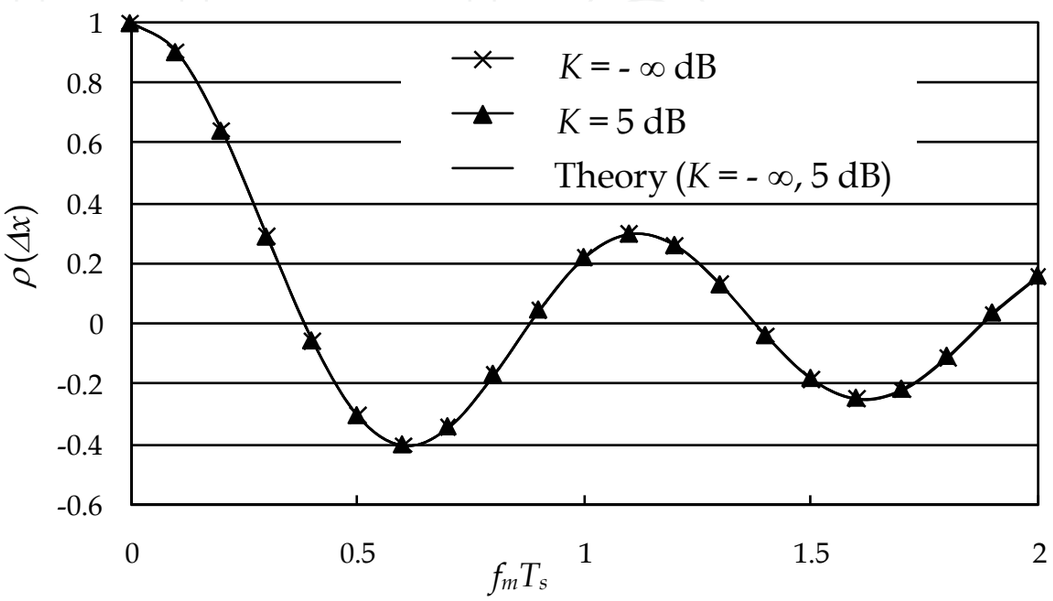

(a) Autocorrelation

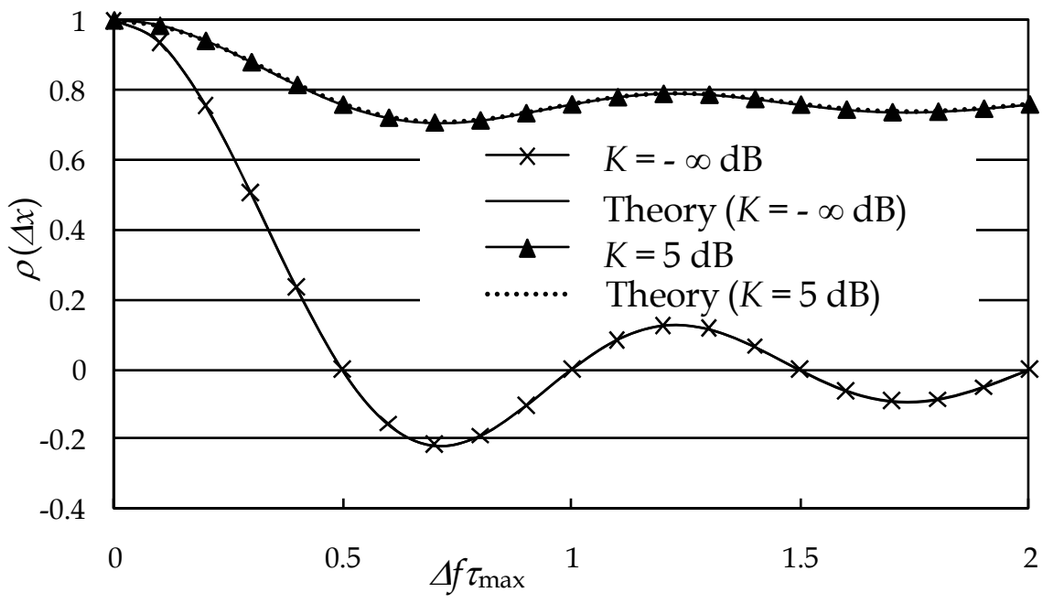

(b) Frequency correlation

Fig. 8. Correlation coefficient (Type 2 : random distribution)

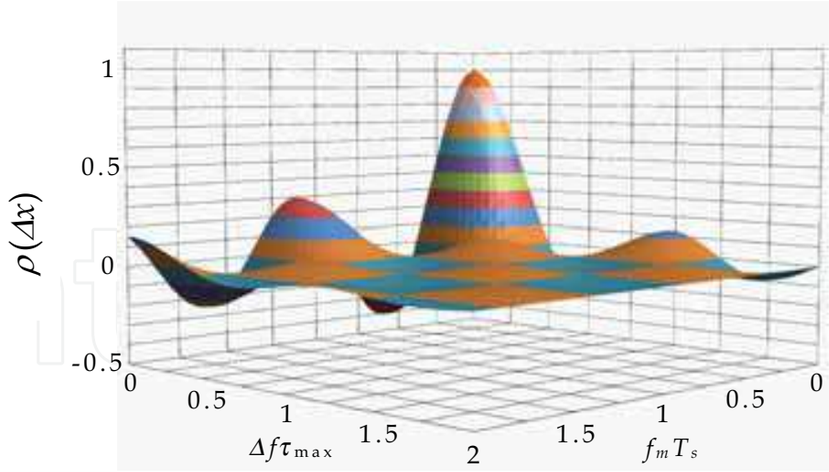

(a) Bird's-eye view (theory)

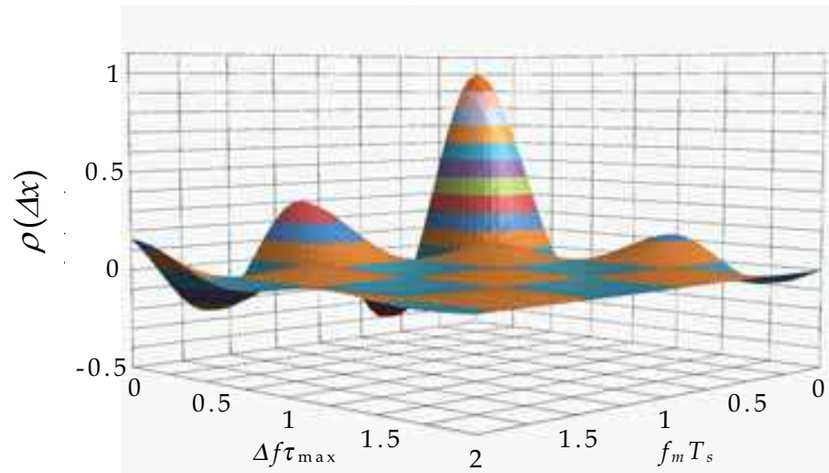

(b) Bird's-eye view (simulation)

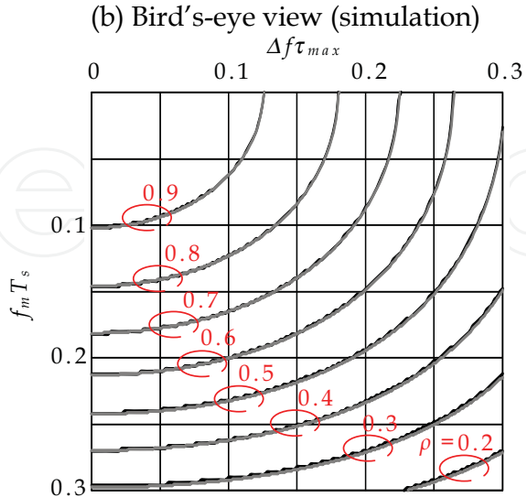

(c) Locus of theory (fine) & simulation (solid)

Fig. 9. Correlation coefficient in a domain with time and frequency axes (Type 2: random distribution , K = -∞ dB)

5. Conclusion

An analysis model having a domain with time, frequency, and space axes was prepared to study the correlation coefficients of the I and Q components in a mobile channel, which are needed in order to allocate a pilot signal with M-ary QAM detection, such as in an OFDM system, and to compose antennas in the MIMO technique. For a multipath environment, the general correlation coefficient formula was derived on the basis of a delay profile with and without a directive wave, and as examples, the formulas for delay profiles with exponential and random distributions were then derived. The formulas exhibit some interesting features: the autocorrelation on the time axis is independent of the K factor and is expressed by $J_0(2\pi f'_m T_s)$, but the frequency correlation depends on the K factor and delay profile type. The locus of a fixed value correlation is an ellipse in the domain with time and frequency axes. The correlations were also shown in the domain using bird's-eye views for easy comprehension. Furthermore, computer simulation was performed to verify the derived formulas and the theoretical and simulated values agree well. Therefore, it is possible to estimate logically the pilot signal allocation of M-ary QAM in OFDM and antenna construction for MIMO in the domain.

6. Appendix

6.1 Appendix A derivation of (8)

Under the conditions of the propagation model in 2-A and assuming that N is a large number, $\langle I(0)I(\Delta x)\rangle$ is analyzed as follows. It is separated into terms of the same ith and other ith arriving waves, as shown in (17).

$$\begin{aligned}\langle I(0)I(\Delta x)\rangle &= \langle[\sum_{i=0}^{N} h_i \cos(2\pi f_c \tau_i + \phi_i)][\sum_{i=0}^{N} h_i \cos\{2\pi((f_c+\Delta f)\tau_i - f_m' T_s \cos\xi_i) + \phi_i\}]\rangle \\ &= \langle \sum_{i=0}^{N} h_i^2 \cos(2\pi f_c \tau_i + \phi_i)\cos\{2\pi((f_c+\Delta f)\tau_i - f_m' T_s \cos\xi_i) + \phi_i\} \\ &\quad + \sum_{i=0}^{N}{}' \sum_{j=0}^{N}{}' h_i h_j \cos(2\pi f_c \tau_i + \phi_i)\cos\{2\pi((f_c+\Delta f)\tau_j - f_m' T_s \cos\xi_j) + \phi_j\}\rangle, \qquad (17)\end{aligned}$$

$$where\ i \neq j\ on\ \sum_{i=0}^{N}{}' \sum_{j=0}^{N}{}'$$

Furthermore, the second term in (17) vanishes because the values of τ_i , ξ_i, and ϕ_i for the ith wave and τ_j, ξ_j, and ϕ_j for the jth wave are independent of each other and are also random values, and the sum of the products of $\cos\theta_i$ and $\cos\theta_j$ then becomes zero. With this in mind and considering the small values of $\Delta f \tau_i$ and $f_m' T_s$, the first term of (17) is modified as (18) to (20) by using, for example, a transforming trigonometric function, τ_i , ξ_i, and ϕ_i with random values, and an odd function of sine. In this procedure, the second terms in (18) and (19) also vanish, so we finally get (20) as the result for $\langle I(0)I(\Delta x)\rangle$.

$$Eq.\ (17) = \langle \frac{1}{2}\sum_{i=0}^{N} h_i^2 [\cos(2\pi(\Delta f \tau_i - f_m' T_s \cos\xi_i)) + \cos\{2\pi((2f_c+\Delta f)\tau_i - f_m' T_s \cos\xi_i) + 2\phi_i\}]\rangle \quad (18)$$

$$= \langle \frac{1}{2} \sum_{i=0}^{N} h_i^2 [\cos(2\pi \Delta f \tau_i) \cos(-2\pi f_m^{'} T_s \cos\xi_i) - \sin(2\pi \Delta f \tau_i) \sin(-2\pi f_m^{'} T_s \cos\xi_i)] \rangle \quad (19)$$

$$= \langle \frac{1}{2} \sum_{i=0}^{N} h_i^2 \cos(2\pi \Delta f \tau_i) \cos(-2\pi f_m^{'} T_s \cos\xi_i) \rangle \quad (20)$$

6.2 Appendix B derivation of (12)

In the first term A_1 in (11), we change A_1 to (21) because the directive wave's amplitude h_0 is usually much larger than that of the nondirective one and because τ_0=0. Moreover, the amplitude h_i of the ith arriving wave depends on excess delay time τ_i according to (10). So by substituting (10) for h_i, we can rewrite (21) as (22).

$$A_1 = \langle \frac{1}{2} [h_0^2 + \sum_{i=1}^{N} h_i^2 \cos(2\pi \Delta f \tau_i)] \ \rangle \quad (21)$$

$$= \langle \frac{1}{2} h_0^2 \rangle + \langle \frac{1}{2} \sum_{i=1}^{N} [h \exp(-\tau_i / \tau_{av})]^2 \cos(2\pi \Delta f \tau_i) \rangle \quad (22)$$

We try to calculate by replacing the ensemble average of the second term in (22) by integration with respect to τ_i assuming a large N. As a result, we get (23) assuming $\tau_{\min}$ is close to 0 and $\tau_{\max}$ is large.

$$A_1 = \langle \frac{1}{2} h_0^2 \rangle + \frac{h^2}{2} \int_{\tau_{\min}}^{\tau_{\max}} \exp(-2\tau / \tau_{av}) \cos(2\pi \Delta f \tau) d\tau$$

$$= \langle \frac{1}{2} h_0^2 \rangle + \frac{h^2 \tau_{av} / 4}{1 + (\tau_{av} / 2)^2 (2\pi \Delta f)^2} \quad (23)$$

Furthermore, we need to adjust h in (23) to a normalized power of 1 when N and $\tau_{\max}$ are large, so we get

$$\sum_{i=1}^{N} \frac{1}{2} h_i^2 = \frac{1}{2} \sum_{i=1}^{N} [h \exp(-\tau_i / \tau_{av})]^2$$

$$= \frac{h^2}{2} \int_{\tau_{\min}}^{\tau_{\max}} \exp(-2\tau / \tau_{av}) d\tau$$

$$= \frac{1}{4} h^2 \tau_{av} = 1. \quad (24)$$

Consequently, the numerator of the second term in (23) should be 1. Furthermore, considering $\left\langle \frac{1}{2} h_0^2 \right\rangle$, we get (25).

$$A_1 = k + \frac{1}{1 + (\tau_{av} / 2)^2 (2\pi \Delta f)^2} \quad (25)$$

6.3 Appendix C derivation of (15)

We calculate the ensemble average of A_2 in (14) in a similar manner to that for (23) by integrating with the provability density function $1/\tau_{\max}$ of τ. Considering the independence of h_i and τ_i and the power of the directive and nondirective waves, or k and 1, we get (26).

$$
\begin{aligned}
A_2 &= \left\langle \ \frac{1}{2}h_0^2 + \frac{1}{2}\sum_{i=1}^{N} h_i^2 \cos(2\pi \Delta f \tau_i) \ \right\rangle \\
&= k + \langle \frac{1}{2}\sum_{i=1}^{N} h_i^2 \rangle \langle \sum_{i=1}^{N} \cos(2\pi \Delta f \tau_i \rangle \\
&= k + \frac{1}{\tau_{\max}} \int_{\tau_{\min}}^{\tau_{\max}} \cos(2\pi \Delta f \tau) d\tau \\
&= k + \frac{\sin(2\pi \Delta f \tau_{\max})}{2\pi \Delta f \tau_{\max}}
\end{aligned}
\tag{26}
$$

7. References

[1] ITU Circular Letter 5/LCCE/2, Radiocommunication Bureau, 7 March 2008.

[2] Richard van Nee and Ramjee Prasad, OFDM FOR WIRELESS MULTIMEDIA COMMUNICATIONS, Artech House, 1999.

[3] T. Hwang, C. Yang, G. Wu, S. Li, and G. Y. Li, OFDM and Its Wireless Applications: A Survey, *IEEE Trans. Veh. Technol.*, Vol. 58, No. 4, pp. 1673-1694, May 2009.

[4] G. J. Foschini and M. J. Gans, On limits of wireless communications in fading environments when using multiple antennas, *Wireless Personal Commun*. Vol. 6, pp. 311-335, 1998.

[5] D. Shiu, G. Foschini, M. J. Gans, and J. Kahn, Fading Correlation and Its Effect on the Capacity of Multielement Antenna Systems, *IEEE Trans. Commun.*, Vol. 48, No. 3, pp. 502-513, March 2000.

[6] Andreas F. Molisch, Martin Steinbauer, Martin Toeltsch, Ernst Bonek, and Reiner S. Thoma, Capacity of MIMO Systems Based on Measured Wireless Channel, *IEEE JSAC*, Vol. 20, No. 3, pp. 561-569, April 2002.

[7] H. Nishimoto, Y. Ogawa, T. Nishimura, and T. Ohgana, Measurement-Based Performance Evaluation of MIMO Spatial Multiplexing in Multipath-Rich Indoor Environment, *IEEE Trans. Antennas and Propag.*, Vol. 55, No. 12, pp. 3677-3689, Dec. 2007.

[8] Seiichi Sampei and Terumi Sunaga, Rayleigh Fading Compensation for QAM in Land Mobile Radio Communications, *IEEE Trans. Veh. Technol.*, Vol. 42, No. 2, pp. 137-147, May 1993.

[9] R. H. Clarke, A statistical theory of mobile-radio reception, *Bell Syst. Tech. J.*, Vol. 47, No. 6, pp. 957-1000, 1968.

[10] William C. Jakes, MICROWAVE MOBILE COMMUNICATIONS, John Wiley & Sons, Inc., 1974.

[11] S. Kozono, T. Tsuruhara, and M. Sakamoto, Base Station Polarization Diversity Reception for Mobile Radio, *IEEE Trans. Veh. Technol.*, Vol. VT33, No. 4, pp. 301-306, Nov. 1984.

[12] H. Nakabayashi and S. Kozono, Theoretical Analysis of Frequency-Correlation Coefficient for Received Signal Level in Mobile Communications, *IEEE Trans. Veh. Technol.*, Vol. 51, No. 4, pp. 729-737, July 2002.

[13] S. Kozono, K. Ookubo, and K. Yoshida, Study of Correlation Coefficients of Complex Envelope and Phase in a Domain with Time and Frequency Axes in Narrowband Multipath Channel, in *69th IEEE Veh. Technol. Conf.*, Barcelona, Spain, April 2009.

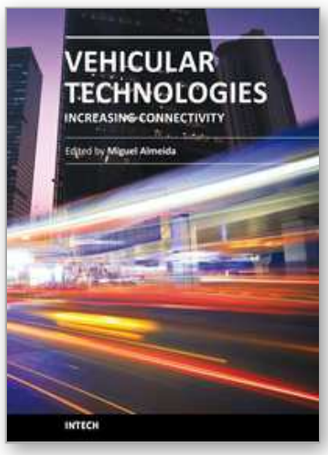

Vehicular Technologies: Increasing Connectivity
Edited by Dr Miguel Almeida

ISBN 978-953-307-223-4
Hard cover, 448 pages
Publisher InTech
Published online 11, April, 2011
Published in print edition April, 2011

This book provides an insight on both the challenges and the technological solutions of several approaches, which allow connecting vehicles between each other and with the network. It underlines the trends on networking capabilities and their issues, further focusing on the MAC and Physical layer challenges. Ranging from the advances on radio access technologies to intelligent mechanisms deployed to enhance cooperative communications, cognitive radio and multiple antenna systems have been given particular highlight.

How to reference
In order to correctly reference this scholarly work, feel free to copy and paste the following:

Shigeru Kozono, Kenji Ookubo, Takeshi Kozima and Tomohiro Hamashima (2011). Correlation Coefficients of Received Signal I and Q Components in a Domain with Time and Frequency Axes under Multipath Mobile Channel with LOS and NLOS, Vehicular Technologies: Increasing Connectivity, Dr Miguel Almeida (Ed.), ISBN: 978-953-307-223-4, InTech, Available from: http://www.intechopen.com/books/vehicular-technologies-increasing-connectivity/correlation-coefficients-of-received-signal-i-and-q-components-in-a-domain-with-time-and-frequency-a

INTECH
open science | open minds

InTech Europe
University Campus STeP Ri
Slavka Krautzeka 83/A
51000 Rijeka, Croatia
Phone: +385 (51) 770 447
Fax: +385 (51) 686 166
www.intechopen.com

InTech China
Unit 405, Office Block, Hotel Equatorial Shanghai
No.65, Yan An Road (West), Shanghai, 200040, China
中国上海市延安西路65号上海国际贵都大饭店办公楼405单元
Phone: +86-21-62489820
Fax: +86-21-62489821

IntechOpen